36H-L.0 ADDITIVE MANUFACTURING OF REFRACTORY MULTIPRINCIPAL ELEMENT ALLOYS

Megan Le Corre (Mines)
Faculty: Amy Clarke (Mines)
Industrial Mentor: TBD

This project initiated in Fall 2021 and is supported by the ONR-MURI Project. The research performed during this project will serve as the basis for a Ph.D. thesis program for Megan Le Corre.

36H-L.1 Project Overview and Industrial Relevance

This project seeks first to determine what impact various additive manufacturing conditions might have on the properties of refractory multi-principal element alloys (RMPEAs). This will be done by conducting single line track melts on solid base material, producing similar solidification conditions as might be experienced during AM. The resulting microstructures from these experiments will then be compared to expected microstructures. Once a baseline understanding of the solidification behavior has been established, methods of microstructural control will be evaluated, and alloys will be tailored for the AM process to ensure optimal behavior under ultra-high temperature operating conditions.

RMPEAs are a relatively new area of metallurgical development, offering unique and tailorable microstructures. The development of these alloys has the potential to produce a full step change in performance when compared to traditionally used nickel-based superalloys, whose performance begins to deteriorate beyond 1100°C. Despite their potential benefits, these alloys have limited workability at lower temperatures and thus are challenging to manufacture by traditional methods such as thermomechanical processing. These formability challenges can be circumvented by use of additive manufacturing methods, whereby a final or near-net shape part can be directly produced one layer at a time. A significant benefit of additive manufacturing lies in that it allows for considerable form freedom and part subcomponent reduction. These features are of particular use in applications requiring complex geometries. The prospective mechanical and thermal properties of RMPEAs combined with the benefits conferred by additive manufacturing provides significant promise for many existing and budding technologies requiring ultra-high operating temperatures. Potential applications include nuclear thermal propulsion (NTP), in-space green propulsion, reusable hypersonic wing leading edges for re-entry thermal protection, and advanced power and propulsion applications, such as fusion.

36H-L.2 Previous Work (literature review)

Multi-principal element alloys (MPEAs), as their name implies, are alloys that are comprised of more than one principal element, which is to say that no one element acts as the base. This class of alloys are also known as high entropy alloys (HEAs) or complex concentrated alloys (CCAs) in literature and in industry [36H-L.1]. In the case of RMPEAs, alloying elements might include tungsten (W), molybdenum (Mo), tantalum (Ta), niobium (Nb), vanadium (V), hafnium (Hf), zirconium (Zf), rhenium (Re), with additions of titanium (Ti) or chromium (Cr) to improve oxidation and corrosion resistance [36H-L.2]. In general, single-phase compositions are desirable and solid solution strengthening is preferred over precipitation strengthening due to the elevated operational temperatures for which these alloys are designed. Previous work by former CANFSA student Dr. F.G. Coury identified four equiatomic RMPEAs in which single phase BCC structure was stable up to 1400 °C; these include HfNbTaTi, MoNbTaTi, WNbTaTi, and CrMoNbTi [36H-L.3]. Two compositions were found to form single-phase B2 crystal structures, namely AlHfNbTi and AlHfTaTi. The solidification behavior of these alloys will be evaluated under simulated AM conditions to determine the feasibility of future component production.

Simulated AM conditions will take the form of single-track laser melts on solid bar, plate, or arc-melted buttons in a similar manner to the experiments conducted by J.D. Roehling et al. [36H-L.4]. In these experiments, laser track melts were performed in Ti-20Nb and Ti-50Nb (at. %). Solidification velocities were calculated from images of the melt tracks and the resulting microstructures were characterized.

Despite the potential benefits that may come with additive manufacturing of RMPEAs, several challenges still exist that will need to be addressed. Melia et al. conducted work evaluating the solidification response of compositionally

graded RMPEAs as well as a compositionally uniform MoNbTaW produced by L-DED (Laser Directed Energy Deposition) [36H-L.5]. It was found that the compositionally uniform MoNbTaW sample showed significant solidification cracking throughout the sample along preferentially oriented <100> grain growth direction. The produced equiatomic sample also showed deviation from desired equiatomic chemistry. The mechanisms responsible for these compositional deviations are not yet fully understood, underlying the need to conduct further research in this field.

36H-L.3 Recent Progress

36H-L.3.1 Solidification Behavior of Nb-47Ti

In addition to the evaluation of the AM solidification behavior of RMPEAs, a select handful of traditional refractory alloys will also be evaluated as part of this project. These will include the binary niobium alloy Nb-47Ti and the more heavily alloyed C103. These current refractory alloys are also of significant interest to industry, and their solidification responses as a result of additive manufacturing conditions are not well understood, but are expected to generate important baseline data that will translate to the processing of RMPEAs. The respective compositions of these alloys can be found in **Table 36H-L.1**. Recent work has most heavily been focused on the evaluation of Nb-47Ti; evaluation of C103 is expected to be conducted before the next reporting period.

The Ivantsov Marginal Stability (IMS) model was used to determine expected dendrite tip radius as a function of solidification velocity [36H-L.6]. Thermo-Calc software was used to produce a single axis simulation to determine required inputs for the IMS model, including liquidus slope, partition coefficient, and liquidus temperature. The diffusion coefficient was approximated assuming substitutional diffusion. The Gibbs-Thompson coefficient was based on the more commonly available value used for nickel-based superalloys. These values are found in **Table 36H-L.2.** The IMS model was also used to determine the relationship between solidification velocity and total undercooling. Planar, cellular, and dendritic growth regions were determined and plotted as a function of solidification velocity (V) and temperature gradient (G). Additionally, the Gaümann columnar-to-equiaxed transition (CET) model was used to determine the G-V boundaries indicating the transition from fully columnar dendritic growth to 1% equiaxed and 50% equiaxed dendritic growth [36H-L.7]. Values used to determine the CET were assumed to be fairly conservative and are found in **Table 36H-L.3**. These boundaries are overlayed on the G-V plot in **Figure 36H-L.1** in Section 31.5.

Three laser track melts were produced using DED parameters as a basis [36H-L.8]. The base material is a forged and annealed bar provided by the CANFSA sponsor ATI. The parameters that were evaluated are found in **Table 36H-L.4**. Spot size was only determined for the third track melt using the method described by Fuerschenbach et al. [36H-L.9], however, given the shorter relative offset distance used for one and two, it is assumed that the spot size for tracks one and two are smaller than that of track three. **Figure 36H-L.2** shows the interior of the laser welding cabinet used to conduct track melts. **Figure 36H-L.3a** shows a top view of a laser melt immediately after removal from the welding cabinet. All three track melts appear to have keyholed, an example of which can be seen in the etched laser track cross section in **Figure 36H-L.3b**. Keyhole mode melting occurs when the targeted material reaches its vaporization temperature; this vaporized metal gas then expands, creating a “keyhole” shape in the material. This mode of melting is generally considered undesirable in welding and additive manufacturing. Additionally, this mode is not accounted for in IMS or CET modeling, thus data collected from types of track melts cannot be used to validate expected growth models. This underlies the need for future track melting efforts to develop parameters that result in conduction mode melting so that resulting material can be used to validate developed G-V curves and the CET regime.

36H-L.3.2 AconityMini Procurement

CANFSA has identified and intends to procure a small L-PBF system that is capable of high pre-heat temperatures (max 800°C). In addition to high temperature capability, the identified system, the AconityMini, has a small build volume, which makes it an excellent choice for the evaluation of expensive or experimental powders. Once procured and delivered, this system will be used to evaluate the effects of pre-heat temperatures on resultant microstructures during printing. It is expected that previously seen solidification cracking can be mitigated using this method.

36H-L.4 Plans for Next Reporting Period

- Develop machine-appropriate laser track melt parameters to validate G-V model.
- Evaluate extent of inter-dendritic microsegregation in laser track melts of Nb-47Ti.
- Model Gaümann modification of the Rosenthal solution for a Gaussian laser intensity profile.
- Evaluate relative extent of oxidation in Nb-47Ti track melts by EDS.
- Produce equivalent evaluation of C103 solidification behavior.

36H-L.5 References

[36H-L.1] D.B. Miracle, O.N. Senkov. A critical review of high entropy alloys and related concepts. Acta Materialia. 122 (2017) 448-511.

[36H-L.2] B. Gorr, M. Azim, H.J. Christ, T. Mueller, D. Schliephake, M. Heilmaier. Phase equilibria, microstructure, and high temperature oxidation resistance of novel refractory high-entropy alloys. Journal of Alloys and Compounds. 624 (2015) 270–278.

[36H-L.3] F.G. Coury, T. Butler, K. Chaput, A. Saville, J. Copley, J. Foltz, P. Mason, K. Clarke, M. Kaufman, A. Clarke. Phase equilibria, mechanical properties and design of quaternary refractory high entropy alloys. Materials & Design. 155 (2018) 244-245.

[36H-L.4] J.D. Roehling, A. Perron, J.-L. Fattebert, T. Haxhimali, G. Guss, T.T. Li, D. Bober, A.W. Stokes, A.J. Clarke, P.E.A. Turchi, M. Matthews, J.T. McKeown. Rapid solidification in bulk Ti-Nb alloys by single track laser melting. Journal of Materials. 70 (2018) 1589-1597.

[36H-L.5] M.A. Melia, S.R. Whetten, R. Puckett, M. Jones, M.J. Heiden, N. Argibay, A.B. Kustas. High-throughput additive manufacturing and characterization of refractory high entropy alloys. Applied Materials Today. 19 (2020) 1-15.

[36H-L.6] R. Trivedi and W. Kurz. Dendritic Growth. International Materials Reviews. 39 (1994) 48-74.

[36H-L.7] J.A. Dantzig, M. Rappaz. Solidification, 2nd Ed. Ecole polytechnique fédérale de Lausanne Press, 2016.

[36H-L.8] J.M. Amado, A. Carballo, J.N. Montero, A. Vicente-Escuder, M.J. Tobar, V. Amigo, A. Yañez. Characterization of TiNb Alloys Obtained in situ by Laser Metal Deposition, European Powder Metallurgy Association. (2021) 1-5.

[36H-L.9] R.C. Dykhuizen, P.W. Fuerschbach, A.R. Mahoney, & J.T. Norris. Development and evaluation of an in-situ beam measurement for spot welding lasers. Welding Journal. (2004) 154-159.

36H-L.6 Figures and Tables

Table 36H-L.1: Nominal Compositions of Nb-47Ti (left) and C103 (right).

Element	Composition [wt. %], Nb-47Ti	Composition [wt. %], C103
Niobium, Nb	53 (balance)	89 (balance)
Titanium, Ti	47	1
Hafnium, Hf	0	10

Table 36H-L.2: Alloy Constants used in IMS model for Nb-47Ti.

Alloy Constants		Solute 1: Ti
Gibbs-Thompson [K m]	Γ	0.00000018
Diffusion Coefficient [m^2/s]	D	0.000000001
Partition Coefficient [unitless]	k	0.713649149
Liquidus Slope [K/wt %]	m	-7.93321
Initial Concentration [wt %]	C_o	47
Liquidus Temperature of Alloy [K]	T_l	2209.70686

Table 36H-L.3: Constants used in CET Model for Nb-47Ti.

CET Constants		1% Equiaxed	50% Equiaxed
Nucleation Site Density [$\#/m^3$]	N_o	$2.2x10^{12}$	$2.2x10^{12}$
Nucleation Undercooling [K]	ΔT_o	2.5	2.5
Volume Fraction of Equiaxed Grains [unitless]	Φ	0.01	0.50

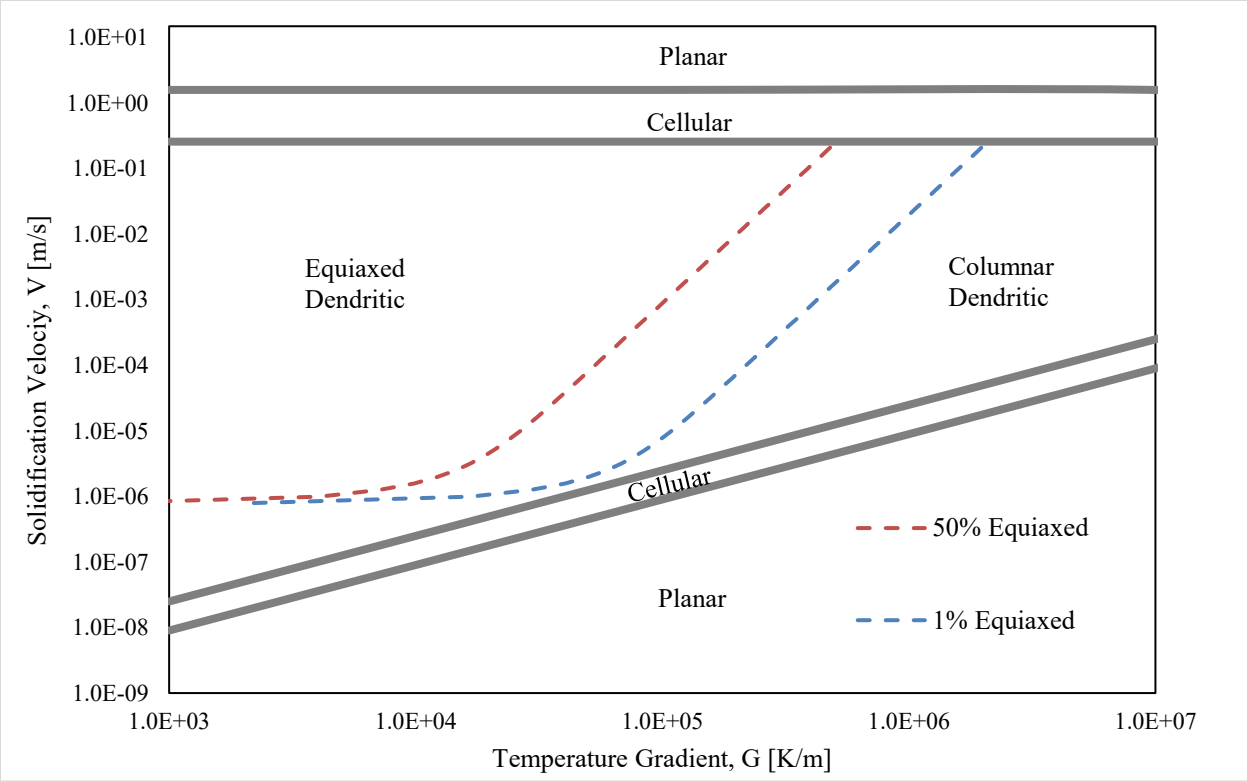

Figure 36H-L.1: Solidification Velocity vs Temperature Gradient (G-V) plot showing regions of planar, cellular, and dendritic growth, including regions of equiaxed dendritic and fully columnar dendritic for Nb-47Ti.

Table 36H-L.4: Process Parameters Used in Laser Track Melts of Nb-47Ti Plate.

	Laser Track 1	Laser Track 2	Laser Track 3
Power [W]	2000	2000	2000
Scan Speed [m/s]	20	20	20
Argon Flow [L/min]	7.08	14.16	20
Spot Size [mm]	(undetermined)	(undetermined)	2

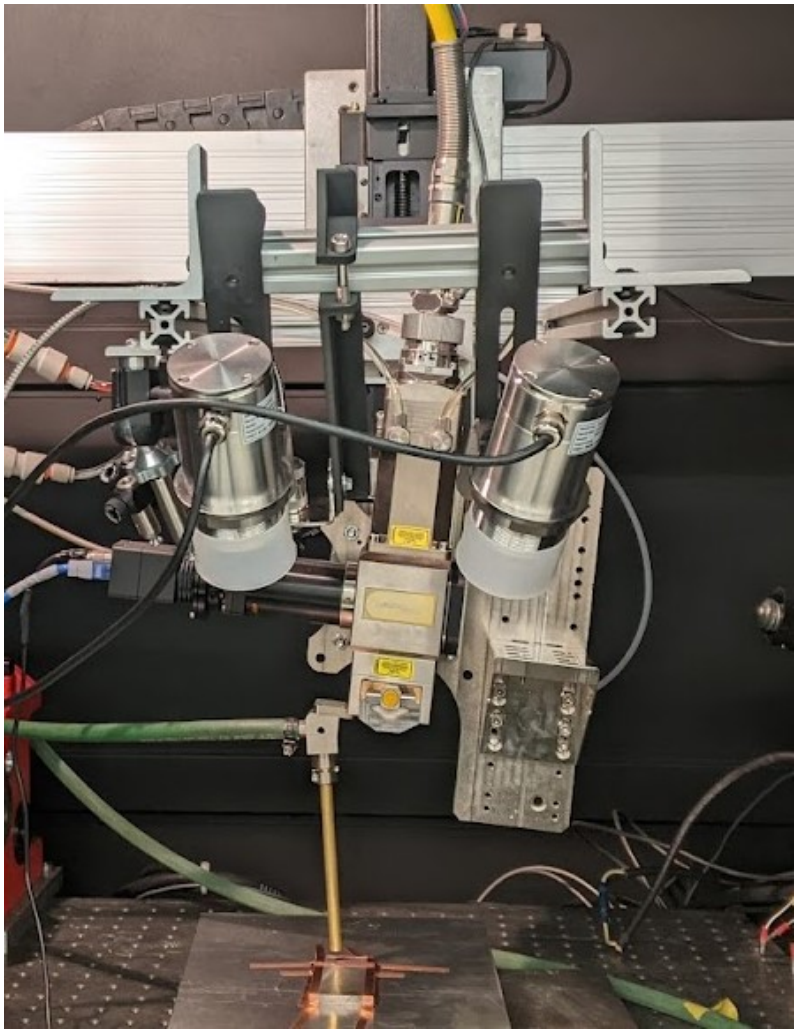

Figure 36H-L.2: Interior of laser welding cabinet with Nb-47Ti sample positioned immediately below Argon delivery tube and collimating optics and fiber optic cable above.

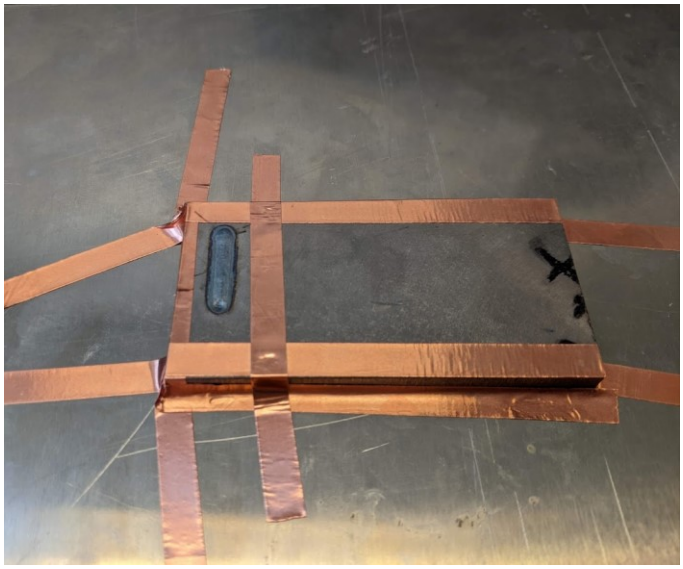

Figure 36H-L.3: A completed track melt outlined with conductive copper tape to improve conductive heat flow away from sample and into aluminum “base plate”. This was done in an effort to simulate “semi-infinite slab” conditions.

Figure 36H-L.4: An LOM image of an etched laser track melt cross section in Nb-47Ti showing significant keyholing, rather than the more desirable conduction-mode melting. Sample was etched with Kroll’s Reagent.